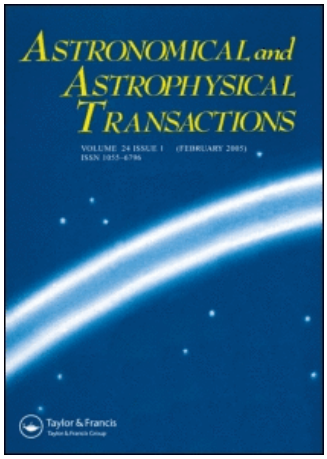

Astronomical & Astrophysical Transactions
The Journal of the Eurasian Astronomical Society
Publication details, including instructions for authors and subscription information:
http://www.informaworld.com/smpp/title~content=t713453505

Geometrical methods of analysis of polarization of CMB

A. D. Dolgov [a]; A. G. Doroshkevich [a]; D. I. Novikov [b]; I. D. Novikov [a]
[a] Theoretical Astrophysics Centre, Copenhagen, Denmark
[b] Theoretische Physik der Universitat Munchen, Munchen, Germany

Online Publication Date: 01 January 2000
To cite this Article: Dolgov, A. D., Doroshkevich, A. G., Novikov, D. I. and Novikov, I. D. (2000) 'Geometrical methods of analysis of polarization of CMB', Astronomical & Astrophysical Transactions, 19:3, 213 - 231
To link to this article: DOI: 10.1080/10556790008238573
URL: http://dx.doi.org/10.1080/10556790008238573

Astronomical and Astrophysical Transactions, 2000, Vol. 19, pp. 213–231
Reprints available directly from the publisher
Photocopying permitted by license only

GEOMETRICAL METHODS OF ANALYSIS OF POLARIZATION OF CMB

A. D. DOLGOV,[1] A. G. DOROSHKEVICH,[1] D. I. NOVIKOV,[2] and I. D. NOVIKOV[1]

[1] *Theoretical Astrophysics Centre, Juliane Maries Vej 30, DK-2100, Copenhagen, Denmark*
[2] *Theoretische Physik der Universitat Munchen, Theresienstr. 37 D-80333 Munchen, Germany*

(Received December 28, 1999)

Future measurements of the polarization of the cosmic microwave background (CMB) are very powerful tools for cosmological studies and may help in extracting cosmological parameters from the observational data. In particular, the polarization is quite sensitive to the presence of primordial gravitational waves.

In this talk we analyse the geometrical and statistical properties of the polarization of the CMB. This analysis was performed in our recent work. Singular points of the vector field which describes CMB polarization are found and classified. A possible signature of primordial gravitational waves in CMB polarization is discussed. We also discuss some other new methods of analysis of CMB anisotropy and polarization.

KEY WORDS CMB, anisotropy, polarization

1 INTRODUCTION

In this paper we review some new methods of the description and analysis of the CMB. The description of the methods of measurements and analysis of CMB anisotropy can be found in refs. [1–6]. Measurements and analysis of the polarization of the CMB allow one to obtain additional cosmological information. A basic description of CMB polarization can be found in papers [7–9], while a more up-to-date development is given in refs. [10–20].

Polarization of CMB is quite sensitive to the presence of tensor perturbations (gravitational waves) and, as was shown in refs. [10–14] a deviation from zero of the so-called pseudoscalar or 'magnetic' part of the polarization would be an unambiguous indication of the presence of gravitational waves. In what follows we will further elaborate this issue and generalize some of the results of ref. [16].

Geometrical properties of the polarization field were actively studied in recent years [13–16]. Important features, which characterize the geometry and topology of polarization, are the types of singularities of the vector flux lines tangent to the direction of maximum polarization [19] (for an earlier paper see ref. [21]). This vector is parallel to one of the eigenvectors of the Stokes matrix and has magnitude equal to the magnitude of the polarization. The points where this vector vanishes, so that no direction is determined, are singular points on the polarization map and the character of the singularity to a large extent determines the relief of the polarization map, even far away from the points of vanishing polarization. The maps simulated in different papers, including ours, demonstrate that the behaviour (topology) of the flux lines of the polarization field at the points where polarization is non-vanishing, is determined by the type of singularity at vanishing polarization. Hence one may draw a conclusion about the types of singular points by studying polarization maps in the regions where the polarization is measurable. The properties of these singular points are discussed in detail in Section 4.

Statistical properties of the anisotropy of the CMB temperature and the CMB polarization are of primary importance for an understanding of their origin. At the present day only two mechanisms of generation of primordial density perturbations are known: inflation and topological defects. The simplest inflationary scenarios predict Gaussian perturbations that results in the Gaussianity of the CMB temperature fluctuations and polarization at the surface of last scattering. Tests of the Gaussian nature of the temperature fluctuations of CMB, together with a study of its polarization, are important probes of inflation. A possible method of testing the Gaussianity of the CMB is a study of the statistics of the singular points discussed in Section 4.4. The same statistical tests may also be useful for discrimination of signal from noise because Gaussian distributions of both temperature fluctuation and polarization generated by noise are rather improbable.

Naselsky and D. Novikov [22], D. Novikov and Jørgensen [23, 24], suggested a topological method of analysis of maps of CMB anisotropy with and without non-Gaussian noise. In this work the authors investigate the topological properties of the $\Delta T/T$ angular distribution caused by the presence of the Doppler-peak in the spectrum of fluctuations and propose the method of percolation and cluster analysis which allows them to detect non-Gaussian noise and to remove it from the observational data.

In the papers [25, 26] we developed the methods of Naselsky and Novikov [22] and Novikov and Jørgensen [23, 24] for the analysis of the global topology of maps of CMB anisotropy and polarization.

This paper summarizes our investigations [31] and [32], and is organized as follows. The basic concepts and notation are introduced in Section 2. In Section 3 a local description of polarization is compared with a non-local one. In Sections 4 and 5 the classification of singular points is discussed. In Section 5 we demonstrate how cluster analysis can be used for the detection of non-Gaussian noise in the experimental maps of CMB anisotropy and polarization. We discuss the results in Section 6.

2 POLARIZATION OF CMB

In this section we will describe some general properties of CMB polarization and present the necessary formalism. This section has an introductory character and to some extent is described in the literature. We make the simplifying assumption that the relevant angular scales are sufficiently small, so that the corresponding part on the sky is almost flat. In this approximation the polarization field on the sky can be considered as a two-dimensional field on the flat (x, y)-plane. The photon polarization is described by the second rank tensor a_{ij} in the plane perpendicular to photon propagation. By definition this tensor is traceless, because the trace part, proportional to the unit matrix, corresponds to zero polarization and can be absorbed in the total intensity of radiation. It is convenient to expand this tensor in terms of the Pauli matrices σ_α, $\alpha = 1, 2, 3$, which form a complete system in 2×2 traceless matrix space:

$$\mathbf{a} = \xi_\alpha \sigma_\alpha. \tag{1}$$

The parameter ξ_2 is equal to the amplitude of circular polarization, which is not generated by Thomson scattering (due to parity conservation), so that it is usually assumed that $\xi_2 = 0$. In this case the matrix $\mathbf{a}$ is symmetric and is determined by two functions:

$$\mathbf{a} = \begin{pmatrix} Q & U \\ U & -Q \end{pmatrix}. \tag{2}$$

The functions Q and U depend upon the coordinate frame; they are components of the tensor a_{ij} and obey the corresponding tensor transformation law:

$$a'_{ij} = T_i^k T_j^l a_{kl}, \tag{3}$$

where the coordinate transformation is given by $x'_i = T_i^k x_k$. In particular under rotation of the coordinate system with

$$\mathbf{T} = \begin{pmatrix} c & s \\ -s & c \end{pmatrix}, \tag{4}$$

where $c = \cos\phi$, $s = \sin\phi$, and ϕ is the rotation angle, the parameters Q and U are transformed as:

$$\begin{aligned} Q' &= Q\cos 2\phi + U \sin 2\phi, \\ U' &= -Q \sin 2\phi + U \cos 2\phi. \end{aligned} \tag{5}$$

It is more convenient in many cases to work with invariant quantities or at least with vectors, whose direction on the polarization map is easy to visualize. There are the following invariants (or what is the same, scalars) that may be constructed from the second-rank tensor. First, of course, is the trace, $\mathrm{Tr}\,\mathbf{a} = a_{ii}$. In this case it is zero. The second invariant is the determinant of the matrix $\mathbf{a}$,

$$\det \mathbf{a} = Q^2 + U^2. \tag{6}$$

The maximum magnitude of polarization is given by $\sqrt{Q^2+U^2}$. The direction of maximum polarization is determined by one of the eigenvectors of the matrix a_{ij} (see e.g. ref. [19]).

These are the well-known algebraic invariants which exist in any space dimensions. One may construct two more invariants, using the vector operator of differentiation. They can be chosen as:

$$S = \partial_i \partial_j a_{ij},$$
$$P = \epsilon_{kj} \partial_k \partial_i a_{ij}, \tag{7}$$

where $j = 1, 2$ and $\partial_i = \partial/\partial x^j$. In terms of Q and U these invariants are expressed as:

$$S = (\partial_1^2 - \partial_2^2) Q + 2\partial_1 \partial_2 U,$$
$$P = (\partial_1^2 - \partial_2^2) U - 2\partial_1 \partial_2 Q. \tag{8}$$

The first scalar invariant exists in any space dimension, while the second pseudo-scalar exists only in two-dimensional space, because of the presence of the antisymmetric pseudo-tensor ϵ_{kj} (analogous antisymmetric tensor in higher dimensions D has D indices). These quantities S and P coincide, up to a scalar factor, with the B and E fields introduced in refs. [10, 12]. In our opinion it is more natural to denote them as S and P to stress their scalar and pseudo-scalar nature and not as electric and magnetic parts of the polarization because these quantities have nothing to do with vectors. In this sense we agree with the terminology of ref. [27] (see also [13, 15]).

An important feature of the pseudo-scalar P is that it vanishes if only scalar perturbations induce polarization in the CMB. In this case the Stokes matrix can be written in terms of the derivatives of one scalar function:

$$a_{ij} = (2\partial_i \partial_j - \delta_{ij} \partial_k \partial_k) \Psi. \tag{9}$$

It is straightforward to check that indeed $P = 0$. We do not share the opinion and/or terminology of refs. [14, 17] where it is stated that the corresponding field does not possess a curl. As has been shown in ref. [19] this is not true and generically the eigenvectors of the Stokes matrix are not curlless. The validity of this general statement can be verified on simple examples. This means in particular that the flux lines of the direction of maximum polarization may have a non-zero vorticity, in contrast to the statement of refs. [14, 17].

If tensor perturbations are non-vanishing, the polarization matrix has the general form determined by two independent functions. As is well known, an arbitrary three-dimensional vector can be expanded in terms of scalar and vector potentials as

$$\boldsymbol{V} = \operatorname{grad} \Phi + \operatorname{curl} \boldsymbol{A}. \tag{10}$$

In two dimensions an arbitrary vector can be expressed as the derivatives of a scalar and a pseudo-scalar:

$$V_j = \partial_j \Phi_1 + \epsilon_{jk} \partial_k \Phi_2. \tag{11}$$

In direct analogy to this, an arbitrary traceless symmetric 2×2-matrix can be presented in terms of scalar and pseudo-scalar potentials as:

$$a_{ij} = (2\partial_i\partial_j - \delta_{ij}\partial^2)\Psi + (\epsilon_{ik}\partial_k\partial_i)\Phi. \tag{12}$$

Of course now the pseudo-scalar P defined in Eq. (7) does not vanish and this property permits us to observe possible tensor perturbations by measurement of the CMB polarization [10–16]. If $\Psi = 0$ then the scalar S vanishes. Unfortunately this does not mean that tensor perturbations dominate because they contribute both to Φ and Ψ.

3 DIFFERENT METHODS OF DESCRIPTION OF THE CMB POLARIZATION

It is an interesting observational problem of which quantity is easier to measure in a noisy background, a differential local or an integrated global one. As was stated in ref. [15] a measurement of an integrated quantity would be much more robust, and correspondingly the field variables S and P (or in the notation of papers [10–12], E and B) were expressed as integrals over all or a part of the sky. We think that the answer to the question of the best observational strategy very much depends on the properties of the noise. For example, if the noise in the polarization field of the CMB is created by point-like sources, chaotically distributed on the sky with mean separation larger than the resolution of the antenna, then the measurement of local differential quantities, as e.g. direct measurements of S and P given by Eq. (7), seems easier. However there may be sources of noise that would be easier to suppress if one measures a quantity which is averaged over the whole (which is not possible) or part of the sky. To this end we re-derive the expressions for integrated S and P (or E and B) presented in ref. [16]. The derivation is presented in great detail because of some disagreement with ref. [16]. The results are very close but we show that the window function may have a more general form even for the same choice of normalization function $N(l^2)$, defined below.

Let us first define the Fourier transformed fields:

$$\tilde{Q}(\boldsymbol{l}) = \int \mathrm{d}^2 y e^{-i\boldsymbol{l}\boldsymbol{y}} Q(\boldsymbol{y}) \tag{13}$$

and the similar one for U. The Fourier transformed scalar and pseudo-scalar fields can be written as

$$\begin{aligned} \tilde{S}_N(\boldsymbol{l}) &= N(l^2) \int \mathrm{d}^2 y e^{-i\boldsymbol{l}\boldsymbol{y}} [Q(\boldsymbol{y}) \cos 2\phi_l + U(\boldsymbol{y}) \sin 2\phi_l], \\ \tilde{P}_N(\boldsymbol{l}) &= N(l^2) \int \mathrm{d}^2 y e^{-i\boldsymbol{l}\boldsymbol{y}} [U(\boldsymbol{y}) \cos 2\phi_l - Q(\boldsymbol{y}) \sin 2\phi_l] \end{aligned} \tag{14}$$

where ϕ_l is the polar angle in the plane of Fourier coordinates $\boldsymbol{l}$. The scalar function $N(l^2)$ is arbitrary. It preserves the scalar or pseudo-scalar property of S and P. For

the definition (7) one has to choose $N(l^2) = l^2$. The definition used in ref. [16] is $N(l^2) = 1$. This means that a non-locality is introduced in coordinate space by the inverse Laplace operator, $1/\partial^2$, that is by the Green's function of the Laplacian.

Now we can make the inverse Fourier transform to obtain the functions S_N and P_N in coordinate space:

$$S_N(x) = \int \frac{d^2l}{(2\pi)^2} N(l^2) \int d^2y e^{il(x-y)} [Q(y)\cos 2\phi_l + U(y)\sin 2\phi_l],$$

$$P_N(x) = \int \frac{d^2l}{(2\pi)^2} N(l^2) \int d^2y e^{il(x-y)} [-Q(y)\sin 2\phi_l + U(y)\cos 2\phi_l] \qquad (15)$$

where ϕ_l is the angle between the vector l and some fixed direction; it is convenient to choose the latter as the direction of the vector x, so that $\phi_l \equiv \phi_{xl}$.

Integration over the directions of the vector l can be done explicitly. To simplify the notation let us introduce

$$\rho = x - y \qquad (16)$$

and three angles $\phi_{l\rho}$, $\phi_{\rho x}$, and ϕ_{xl} between the directions of the indicated vectors. Evidently

$$\phi_{l\rho} + \phi_{\rho x} + \phi_{xl} = 0. \qquad (17)$$

The angular integral is reduced to

$$\int_0^{2\pi} d\phi_{l\rho} e^{il\rho\cos\phi_{l\rho}} (A\cos 2\phi_{l\rho} + B\sin 2\phi_{l\rho}), \qquad (18)$$

where the coefficient functions A and B do not depend on $\phi_{l\rho}$. The second term vanishes, while the first one gives

$$\int_0^{2\pi} d\phi_{l\rho} e^{il\rho\cos\phi_{l\rho}} \cos 2\phi_{l\rho} = -2\pi J_2(l\rho), \qquad (19)$$

where $J_2(z)$ is the Bessel function (see e.g. [28]).

The integration over the magnitude of l depends upon the form of the function $N(l^2)$ and the result is a function of the magnitude of the vector ρ:

$$\int_0^{\infty} dl l N(l^2) J_2(l\rho) = F_N(\rho). \qquad (20)$$

For the particular case of $N(l^2) = 1$ chosen in ref. [16] the integral can be taken as follows. It is formally divergent so some regularization procedure should be applied. This can be achieved by introducing a small imaginary part to l to ensure convergence (in other words, we have to shift the contour of integration to the upper l-half-plane). Using the relation [28]:

$$zJ_2(z) = J_1(z) - zJ_1'(z) \qquad (21)$$

and integrating by parts, we obtain:

$$F_1(\rho) = \frac{1}{\rho^2}\int_0^\infty \mathrm{d}z z J_2(z)$$
$$= \frac{1}{\rho^2}\left[2\int_0^\infty \mathrm{d}z J_1(z) - zJ_1(z)\Big|_0^\infty\right] = \frac{2}{\rho^2}. \tag{22}$$

Now taking all the contributions together we obtain:

$$S_N(\boldsymbol{x}) = \frac{1}{2\pi}\int_0^\infty \mathrm{d}\rho\rho F_N(\rho)$$
$$\times \int_0^{2\pi} \mathrm{d}\phi[Q(\boldsymbol{x}-\boldsymbol{\rho})\cos 2\phi + U(\boldsymbol{x}-\boldsymbol{\rho})\sin 2\phi],$$
$$P_N(\boldsymbol{x}) = \frac{1}{2\pi}\int_0^\infty \mathrm{d}\rho\rho F_N(\rho)$$
$$\times \int_0^{2\pi} \mathrm{d}\phi[-Q(\boldsymbol{x}-\boldsymbol{\rho})\sin 2\phi + U(\boldsymbol{x}-\boldsymbol{\rho})\cos 2\phi]. \tag{23}$$

For the particular case of $F_N(\rho) = F_1(\rho) = 2/\rho^2$ considered in ref. [16] we obtain almost the same result as the quoted paper with the only difference that we do not see any reason to assume that the window function $F_1(\rho) = 2/\rho^2$ should be taken to be zero at $\rho = 0$. Anyhow, this difference has zero measure and does not have any impact on the value of the integrals (23). Hence it may be disregarded. What, as we think, is more essential is the statement of ref. [16] that in order to avoid difficult (or even impossible) integration of the data over the whole sky one may use a modified window function:

$$F_{sz}(\rho) = -g(\rho) + \frac{2}{\rho^2}\int_0^\rho \mathrm{d}\rho'\rho' g(\rho') \tag{24}$$

with the function $g(\rho)$ subject to the condition:

$$\int \mathrm{d}\rho\rho g(\rho) = 0, \tag{25}$$

where the last integral is taken over all the sky.

We believe that any window function can be used and no additional conditions are necessary. To show that we calculate the functions $S_N(\boldsymbol{x})$ and $P_N(\boldsymbol{x})$ for the particular case of scalar perturbations when the Stokes matrix is given by expression

(9). Calculation of derivatives in polar coordinates is straightforward and after some algebra we obtain:

$$S_N(\boldsymbol{x}) = \frac{1}{2\pi}\int_0^\infty \mathrm{d}\rho\rho W(\rho)\int_0^{2\pi}\mathrm{d}\phi\left(\Psi_{\rho,\rho}(\boldsymbol{x}-\boldsymbol{\rho}) - \frac{\Psi_\rho(\boldsymbol{x}-\boldsymbol{\rho})}{\rho}\right),$$

$$P_N(\boldsymbol{x}) = \frac{1}{2\pi}\int_0^\infty \mathrm{d}\rho\rho W(\rho)\int_0^{2\pi}\mathrm{d}\phi\left(\frac{2\Psi_{\rho,\phi}(\boldsymbol{x}-\boldsymbol{\rho})}{\rho} - \frac{2\Psi_\phi(\boldsymbol{x}-\boldsymbol{\rho})}{\rho^2}\right), \qquad (26)$$

where sub-ρ or sub-ϕ means differentiation with respect to the corresponding variable and $W(\rho)$ is an arbitrary window function.

One can see from the second of these expressions that indeed P vanishes for any window function. Thus to prove the absence of tensor perturbations, one should either observe the vanishing of the local quantity $P(\boldsymbol{x})$ given by Eq. (8) or of the non-local one given by Eq. (26) with an arbitrary convenient window function $W(\rho)$. Which method would be more efficient depends upon the properties of the noise.

4 SINGULAR POINTS IN THE CMB POLARIZATION MAPS

4.1 Introductory Remarks

The polarization state of photons of the CMB can be described by the direction of maximum polarization and its magnitude; the former is parallel to the eigenvector of the Stokes matrix and the latter is equal to $\sqrt{Q^2+U^2}$. Polarization maps simulated in different papers present the corresponding vector field on the two-dimensional plane. For the analysis of the flux lines on this map it is very important to know the properties of the singular points of this vector field. This has been done in ref. [19] and ref. [25] (see also [21]). Another approach was taken in refs. [15, 16] where the properties of the flux lines were analysed in terms of basis functions of tensor spherical harmonics (see Figure 1 in refs. [15, 16]). However the flux lines of these basic functions are quite different from the behaviour of the flux lines of the polarization vector. Of course the analysis in terms of tensor harmonics and the behaviour of the Stokes parameters Q and U can be used for the description of polarization maps but the analysis in terms of eigenvectors of the Stokes matrix permits us to make a more direct description of the properties of the polarization field. Possible types of different singular points as well as their statistical distributions may bring new information about the properties of the CMB. Of course a measurement of CMB polarization near the point where it vanishes is a very difficult observational problem. However it is not necessary to go exactly to the point where $Q^2+U^2=0$. The type of singularity can be determined by the pattern created by the flux lines in the region where the polarization is non-vanishing (see an example of a simulated polarization map below in Figure 4).

The analysis of singular points of the polarization vector field was performed in refs. [19, 21, 25]. It was found in [19] that their types do not fit the well-known classification of singular points of vector fields in the standard theory of dynamical systems. Due to the non-analytic behaviour of the eigenvectors near the zero points, $Q^2 + U^2 = 0$, the separatrices end at the singularity, while in the usual case they smoothly continue through these points. This unusual behaviour, found in our paper [19], is well observed in the polarization maps simulated in refs. [16] and in the map of our paper below (Figure 2). In this section we present a further development of the analysis of our previous paper [19].

4.2 Basic Equations

The eigenvectors of the polarization matrix (2) are:

$$\begin{aligned} \boldsymbol{n}^+ &\sim \{U, \lambda - Q\}, \\ \boldsymbol{n}^- &\sim \{-U, \lambda + Q\}, \end{aligned} \tag{27}$$

where $\lambda = \sqrt{Q^2 + U^2}$ is the magnitude of the eigenvalue and the vectors $\boldsymbol{n}^+$ correspond respectively to the positive and negative eigenvalues, $\pm\lambda$. The vector $\boldsymbol{n}^+$ is parallel to the direction of the maximum polarization, while $\boldsymbol{n}^-$ goes along the direction of the minimal polarization. This is evident in the basis of eigenvectors where the polarization matrix is diagonal, $\mathbf{a} = \mathrm{diag}\{\lambda, -\lambda\}$. The total intensity of light polarized along $\boldsymbol{n}^+$ is given by $I_\pm = I_0 \pm \lambda$. Thus the intensity along $\boldsymbol{n}^+$ is bigger.

For definiteness we will consider the field of directions of the vector $\boldsymbol{n}^+$ and the singular points in this field. The problem of singular points of a vector field $\boldsymbol{V}$ is investigated for the case when the direction of this two-dimensional vector field with components $[x(t), y(t)]$ is governed by the equation

$$\frac{\mathrm{d}y}{\mathrm{d}x} = \frac{F_1(x,y)}{F_2(x,y)}. \tag{28}$$

Singularities may appear if simultaneously both functions $F_{1,2}(x,y)$ vanish. In this case the condition of uniqueness of the solution of the differential equation is not fulfilled and more than one integral curve may pass through the same point. The standard theory is developed for the case when the functions $F_{1,2}$ are analytic near these zeroes, and their first-order Taylor expansion has the form:

$$F_j = a_j(x - x_0) + b_j(y - y_0). \tag{29}$$

The following three singular points are possible in this case: knots, saddles, and foci (see e.g. [29]). The separatrices of the solutions are two intersecting lines, which are simply straight lines in the linear approximation.

However in the case of the polarization vector field the basic equation has the form:

$$\frac{\mathrm{d}y}{\mathrm{d}x} = \frac{n_y^+}{n_x^+} = \frac{\lambda - Q}{U}. \tag{30}$$

The singular points may appear, as above, if both numerator and denominator vanish. This is equivalent to the condition $Q = U = 0$. An essential difference to the standard case is that now the numerator is not analytic near zero. This fact results in a quite different behaviuor of the integral curves near these points. The standard theory is not applicable to this case and below we will investigate the structure of solutions in the vicinity of these points directly. We assume that the functions Q and U are analytic near the points where $Q = U = 0$, so that they can be expanded as:

$$\begin{aligned} Q &\approx q_1 x + q_2 y, \\ U &\approx u_1 x + u_2 y. \end{aligned} \tag{31}$$

For the sake of brevity we assume that Q and U vanish at $x = y = 0$.

4.3 Types of Singular Points

It is convenient to introduce the new coordinates:

$$\begin{aligned} \xi &= q_1 x + q_2 y, \\ \eta &= u_1 x + u_2 y. \end{aligned} \tag{32}$$

Since this coordinate transformation corresponds to a rotation and rescaling of the coordinates, the forms of singular points would remain the same. Now we introduce polar coordinates on the plane (ξ, η):

$$\xi = r\cos\phi, \quad \eta = r\sin\phi. \tag{33}$$

In these coordinates Eq. (30) is rewritten as

$$\frac{\mathrm{d}\ln r}{\mathrm{d}\phi} = \frac{N}{D} \equiv \frac{q_2 t^3 + (q_1 - 2u_2)t^2 - (q_2 + 2u_1)t - q_1}{u_2 t^3 + (u_1 + 2q_2)t^2 + (2q_1 - u_2)t - u_1}, \tag{34}$$

where $t = \tan(\phi/2)$.

In the general case the denominator D has three roots t_j, $j = 1, 2, 3$. Without loss of generality we may assume that $u_2 = 1$. Then these roots satisfy the conditions:

$$\begin{aligned} t_1 t_2 t_3 &= u_1, \\ t_1 t_2 + t_2 t_3 + t_3 t_1 &= 2q_1 - 1, \\ t_1 + t_2 + t_3 &= -(u_1 + 2q_2). \end{aligned} \tag{35}$$

The integration of Eq. (34) becomes straightforward if we expand the r.h.s. in elementary fractions:

$$\frac{\mathrm{d}\ln r}{\mathrm{d}\phi} = q_1 + \sum_j^3 \frac{B_j}{t - t_j}, \tag{36}$$

where, as one can easily see, $B_j = N(t_j)/(t_j - t_k)(t_j - t_l)$, and none of j, k, l are equal to any of the others. It is straightforward to verify that

$$B_1 = -\frac{(1 + t_2 t_3)(1 + t_1^2)^2}{2(t_1 - t_2)(t_1 - t_3)}. \tag{37}$$

The remaining parameters B_2 and B_3 are obtained by cyclic permutations.

Since $\mathrm{d}\ln r/\mathrm{d}\phi = (\mathrm{d}\ln r/\mathrm{d}t)(1 + t^2)/2$ the equation can be finally rewritten as

$$\frac{\mathrm{d}\ln r}{\mathrm{d}t} = \frac{2}{1 + t^2}\left(q_1 + \sum_j^3 \frac{B_j}{t - t_j}\right) \tag{38}$$

and the integration becomes straightforward. The corresponding solution is:

$$r = r_0(1 + t^2)\prod_j^3 (t - t_j)^{2\nu_j}, \tag{39}$$

where r_0 is an arbitrary constant and the powers ν_j are

$$\nu_j = \frac{B_j}{1 + t_j^2} \tag{40}$$

with the constants B_j given by Eq. (37). It can be checked that ν_j satisfy the following conditions:

$$\sum_j^3 \nu_j = -1, \tag{41}$$

$$\sum_j^3 \nu_j t_j = -\frac{1}{2}\left(\sum_j^3 t_j + \prod_j^3 t_j\right) = q_1, \tag{42}$$

$$\prod_j^3 \nu_j = \frac{(1 + t_1^2)(1 + t_2^2)(1 + t_3^2)}{8(t_1 - t_2)^2(t_2 - t_3)^2(t_3 - t_1)^2}(1 + t_1 t_2)(1 + t_2 t_3)(1 + t_3 t_1). \tag{43}$$

The last three factors in Eq. (43) are proportional to the determinant $d = q_1 u_2 - q_2 u_1$:

$$(1 + t_1 t_2)(1 + t_2 t_3)(1 + t_3 t_1) = \frac{2(q_1 u_2 - u_1 q_2)}{u_2^2} \equiv \frac{2d}{u_2^2}. \tag{44}$$

If all the roots t_j are real, then the sign of the product $\prod_j^3 \nu_j$ is the same as the sign of the determinant d. If however one of the roots, e.g. t_1, is real and the other two are complex conjugate, the sign of the determinant and of the product (43) are opposite.

Now we can make the classification of the singular points. Let us first consider the case when all the roots t_j are real. The behaviour of the solution is determined

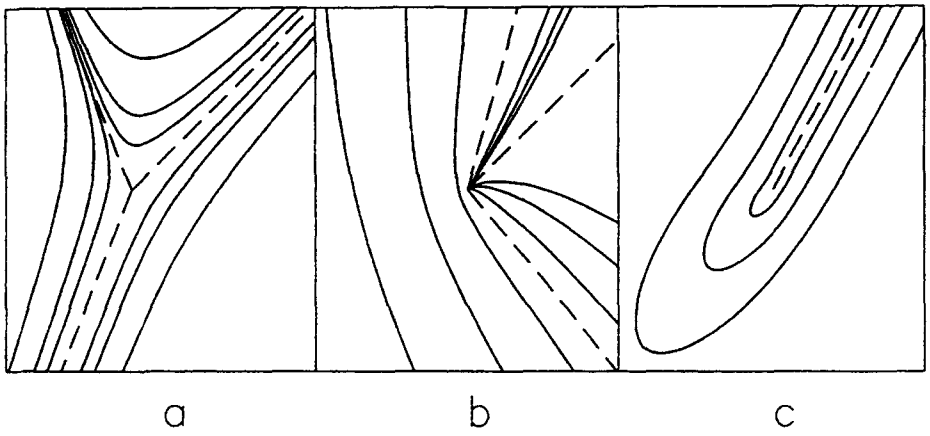

Figure 1 Flux lines for three different types of singular points: (a) saddle, (b) beak, and (c) comet. Dashed lines show peculiar solutions (separatrices).

by the signs of the powers ν_j. Due to Eq. (41) at least one of the powers ν_j must be negative. To see what other signs are possible let us assume (without loss of generality) that

$$t_1 > t_2 > t_3. \tag{45}$$

In this case the following sign relations are valid:

$$\begin{aligned} \text{sign}\,[\nu_1] &= \text{sign}\,[-(1 + t_2 t_3)], \\ \text{sign}\,[\nu_2] &= \text{sign}\,[(1 + t_1 t_3)], \\ \text{sign}\,[\nu_3] &= \text{sign}\,[-(1 + t_1 t_2)]. \end{aligned} \tag{46}$$

If e.g. $t_3 > 0$, the following signs of ν_j are realized $(-,+,-)$. If $t_3 < 0$ but $t_2 > 0$, then $\nu_3 < 0$ and one or both of ν_1 and ν_2 are negative. They cannot both be positive because if $(1 + t_1 t_3) > 0$, then $(1 + t_2 t_3) > 0$ too and $\nu_1 < 0$. Analogously, in the case $t_1 > 0$ and $t_2 < 0$ the set of signs $(-,+,+)$ for any sequence of ν_j is impossible. In the case when all t_j are negative, the sign pattern is $(-,+,-)$. Thus only two sign combinations for ν_j are possible: $(-,-,-)$ and $(-,-,+)$. The first one is realized when $d < 0$ in accordance with expressions (43) and (44). If the determinant is positive, then the signs of ν_j are $(-,-,+)$.

In the case when $d < 0$ the solution does not pass through zero in the vicinity of the singular point. Its behaviour is similar to the usual saddle with the only difference that there are three and not four, as in the usual case, linear asymptotes/separatrices (see Figure 1*a*). We will also call it a 'saddle'. The fact that in our case separatrices are not continued through the singular point, in contrast to the usual singularities, is related to the non-analytic behaviour of Eq. (30) due to the square root singularity.

If $d > 0$, then the sign pattern is $(-,-,+)$ and the solution vanishes along one of the directions and tends to infinity along the other two. The form of the solution

is quite different from the standard ones. The field line cannot be continued along $\phi = \phi_1$ into $\phi = \phi_1 + \pi$ as can be done in the usual case. We will call this type of singularity a 'beak' (see Figure 1*b*).

If only one of the roots t_j is real and the other two are complex conjugate, the solution has the form:

$$\frac{r}{r_0} = (t^2 + 1)|t - t_2|^{4\mathrm{Re}\nu_2} \exp(4\beta \mathrm{Im}\nu_2)(t - t_1)^{2\nu_1}, \tag{47}$$

where $\beta = \tan^{-1}[\mathrm{Im}\, t_2/(t - \mathrm{Re}\, t_2)]$. The real root ν_1 is negative, as is seen from Eq. (43) and thus r does not vanish in the vicinity of such a singular point. The flux lines of the polarization field for this case are presented in Figure 1*c*. This type of singularity can be called a 'comet'. This case is realized when the determinant d is positive.

4.4 Probabilities of Various Types of Singularities

The relative weights of different singular points was calculated in the following way. It is evident that the probability of 'saddles' is 50% because saddles appear if and only if $d < 0$. The probability of comets and beaks was found numerically from the conditions that $d > 0$ and there is a single real root of the equation $D = 0$ (for comets) or there are three real roots (for beaks), where D is the denominator in the expression (34). The probability of the appearance of saddles, beaks and comets for a random choice of q_1, q_2, u_1, and u_2, is correspondingly $W_\mathrm{s} = 0.500$, $W_\mathrm{b} \approx 0.116$, $W_\mathrm{c} \approx 0.384$.

One can also estimate the number density of the singular points in the following way (see e.g. [9, 21]). All singular points correspond to the case when both $Q = 0$ and $U = 0$. The number density of these points is proportional to

$$\mathrm{d}Q\, \mathrm{d}U = |d|\, \mathrm{d}x\, \mathrm{d}y \tag{48}$$

and thus the density is given by the average value of the determinant, $d = q_1 u_2 - q_2 u_1$. It can be shown that saddles make up 50% of all singular points $\langle n_\mathrm{s} \rangle = 0.5\langle n \rangle$, where n is the number density of all singular points. Calculations of the number density of beaks and comets are more complicated and should be done numerically. According to our estimates the surface densities for beaks and comets are correspondingly $\langle n_\mathrm{b} \rangle \approx 0.052\langle n \rangle$ and $\langle n_\mathrm{c} \rangle \approx 0.448\langle n \rangle$. Deviations from these and the above-found numbers for $W_{\mathrm{s,b,c}}$ may signal deviations from the Gaussian nature of the perturbations.

5 CLUSTER ANALYSIS

5.1 Global Topology of Polarization: Cluster Analysis

In this section following the work [26] we investigate some special peculiarities of the CMB polarization, using the method of cluster analysis of maps, refs. [22, 24, 26]. In

order to investigate the global topology of the 10° square anisotropy $\Delta_T(\theta_x, \theta_y)$ and polarization $Q(\theta_x, \theta_y)$ and $U(\theta_x, \theta_y)$ maps, we generated independent realizations of Gaussian processes. We denote $\alpha \equiv \Delta T/\sigma_A$, where σ_A^2 is the variance of the anisotropy of the CMB, and analogous notation for the polarizations Q and U.

In order to give the qualitative characteristics of anisotropy and polarization we made the cross-section of Δ_T, Q and U maps at identical levels of α. We can define a cluster of length k as a collection of k maxima within the closed line of cross-level α [22]. If the value α is high ($\sim$ 2.5–3) the closed lines of levels contain only high maxima of the field. All maxima are separated and only clusters of length $k = 1$ are observed. The reduction of the level α leads to the appearance of big clusters, when the maxima of the clusters begin to connect together and to generate new clusters.

For the values $a \to 0$ the length of clusters $k \to \infty$ and we have the effect of percolation.

In refs. [22–24] it was shown that the rate of clusterization in the anisotropy maps depends very sensitively on the characteristics of possible non-Gaussian noise in a signal. Therefore, the investigation of the cluster statistics is another clue that could have great potential for probing the nature of signals of the sky.

Let us introduce the number of clusters $N_k(\alpha)$ of the length k and the total number of clusters $N(\alpha)$ which are presented in the anisotropy and polarization maps for an appropriate cross-level α:

$$N(\alpha) = \sum_{k=1}^{\infty} N_k(\alpha). \tag{49}$$

We are interested in the mean length of a cluster α[20]:

$$\langle k(\alpha) \rangle = \frac{\sum_{k=1}^{\infty} k N_k(\alpha)}{N(\alpha)} \tag{50}$$

for the whole region considered in the anisotropy and polarization maps.

In Figure 2 we plot the functions $\langle k_T(\alpha) \rangle$, $\langle k_Q(\alpha) \rangle$, $\langle k_U(\alpha) \rangle$ for the Δ_T, Q and U components of polarization, respectively. As one can see from Figure 2, if $|\alpha| < 2$ then the rate of clusterization in the polarization maps is less than in the anisotropy maps.

5.2 Detection of Non-Gaussian Noise in the Maps of Anisotropy and Polarization

The idea that the mean length of a cluster of the CMB anisotropy depends very sensitively on the signal-to-noise ratio was discussed in [22–25]. In this section we demonstrate the applications of cluster analysis for the maps of anisotropy and polarization of the CMB which contain the primordial (Gaussian) signal and non-Gaussian noise. As an example we consider the development of a model (see refs. [23–25]) for non-Gaussian noise. Namely, we consider a regular net of points sources with polarized radiation. The separation of knots of the net is $\theta = 30'$ in the θ_x

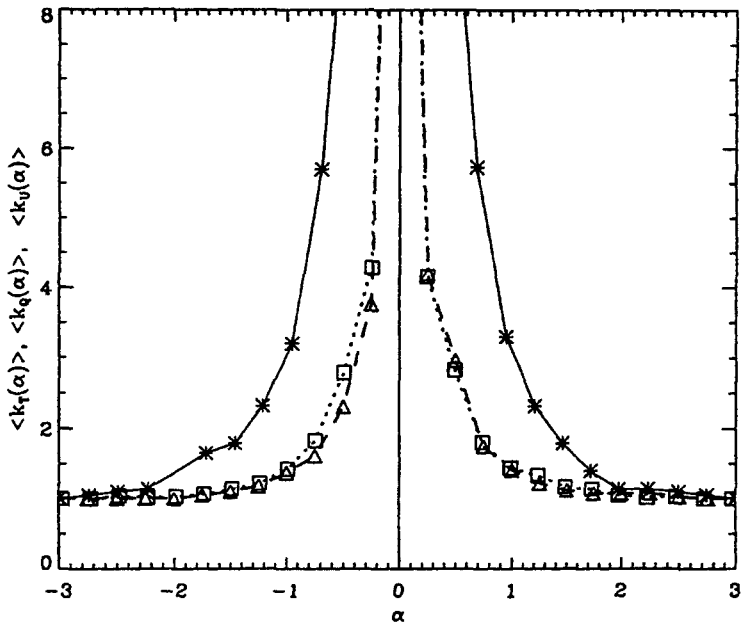

Figure 2 The mean length of clusters of anisotropy $\langle k_T(\alpha)\rangle$ and the Q and U components of polarization. Asterisks correspond to $\langle k_T(\alpha)\rangle$; Δ are the Q and U components of polarization respectively.

and θ_y directions. The angular resolution of the antenna is $6'$. We assume that the intensities of the point sources are random and produce an additional anisotropy uniformly distributed around the mean value δ_n. In this case the distribution of the CMB fluctuations of temperature in the map is:

$$\Delta T_r(\theta_x, \theta_y) = \Delta T_0(\theta_x, \theta_y) + \Delta T_n(\theta_x, \theta_y), \tag{51}$$

where $\Delta T_0(\theta_x, \theta_y)$ is the primordial (Gaussian) signal and $\Delta T_n(\theta_x, \theta_y)$ is the net of sources of noise. Note that the primordial signal and $\Delta T_n(\theta_x, \theta_y)$ are independent of each other and therefore uncorrelated. Besides that, due to the presence of non-Gaussian noise the mean value of $\Delta T_r(\theta_x, \theta_y)$ corresponds to the mean value of the amplitude of the noise δ_n. Let us introduce the new field $\overline{\Delta T}_r(\theta_x; \theta_y)$:

$$\overline{\Delta T}_r(\theta_x, \theta_y) = \Delta T_r(\theta_x, \theta_y) - \delta_n \tag{52}$$

which has the following characteristics:

$$\langle \overline{\Delta T}_r(\theta_x, \theta_y)\rangle_S = 0 \tag{53}$$

and

$$\bar{\sigma}_r^2 = \sigma_A^2 + \sigma_n^2 - \delta_n^2 = \sigma_A^2(1 + a), \tag{54}$$

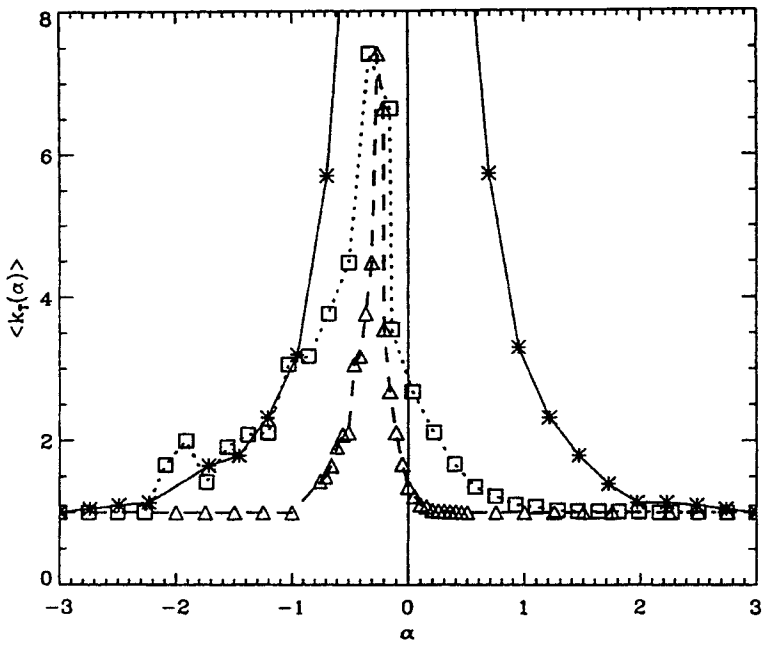

Figure 3 The mean length of clusters of anisotropy without (asterisks and solid line) and with (Δ lines) non-Gaussian noise. Line corresponds to the $a = 0.04$ model; Δ-line corresponds to the $a = 1$ model.

where σ_A is the variance of the primordial signal, σ_n^2 is the variance of the noise, $a = (\sigma_n^2 - \delta_n^2)/\sigma_A^2$ and the brackets $\langle\rangle$ denote averaging over the whole maps.

Now we will discuss the model of non-Gaussian noise of the polarization. We assume that each point source of non-Gaussian noise automatically produces a distortion of two components of polarization. In this case the distribution of the Q and U components of polarization in the map is the following:

$$\begin{pmatrix} Q_r(\theta_x, \theta_y) \\ U_r(\theta_x, \theta_y) \end{pmatrix} = \begin{pmatrix} Q_0(\theta_x, \theta_y) \\ U_0(\theta_x, \theta_y) \end{pmatrix} + b\Delta T_n(\theta_x, \theta_y) \begin{pmatrix} \sin\Psi \\ \cos\Psi \end{pmatrix}, \tag{55}$$

where Q_0 and U_0 are the primordial signals of the polarization, $b = \text{const}$ is the degree of polarization for each source, and Ψ is a random phase homogeneously distributed in the interval $[0, 2\pi]$ (We suppose that the degree of polarization $b = \text{const}$ is the same for all sources). As one can see from (55) the average value of Q_r and U_r is equal to zero, and the parameters $\sigma_{p,n}^2 = (1/2)b^2\sigma_n^2$, $\sigma_Q^2 = \sigma_U^2 = (1/2)\sigma_p^2$ denote the variance of the noise and variances of the Q_0 and U_0 components of the primordial signal. Here σ_p is the total variance of the polarization. The parameter

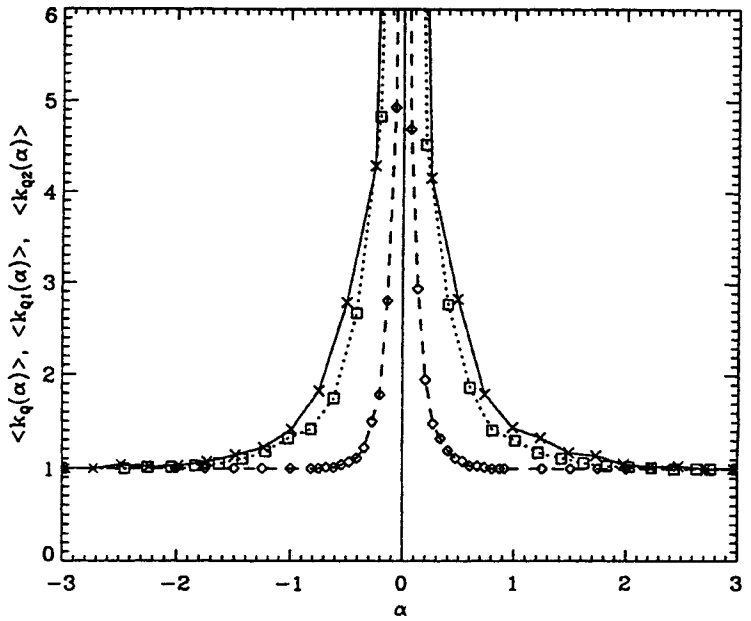

Figure 4 The mean length of clusters for the Q component of polarization with (Δ-lines) and without (asterisks) non-Gaussian noise. Line corresponds to the $p = 0.04$ model; Δ-line corresponds to the $p = 1$ model.

$p = \sigma^2_{p,n}/\sigma^2_Q$ determines the level of the noise in the map of the polarization. Now let us introduce the degree of polarization in the maps without non-Gaussian noise:

$$P = \frac{\sigma^2_p}{\sigma^2_A}. \tag{56}$$

Using (55) and (56) one can write:

$$p = \frac{ab^2P^{-1}}{[1 - (\delta^2_n/\sigma^2_n)]}. \tag{57}$$

If $b^2 = [1 - (\delta^2_n/\sigma^2_n)]P$, then $p = a$ and the levels of noise in the maps of the anisotropy and polarization are practically identical.

In Figures 3 and 4 we plot the dependence of the mean length of the clusters on a cross-level α for four models: $a = 0.04$, $p = 0.04$ and $a = 1$, $p = 1$ and $\delta_n \simeq 0.2\sigma_A$ in both models. These models illustrate the character of the rate of clusterization in the case when non-Gaussian noise is small as for anisotropy and polarization; and vice versa, if the level of the noise is comparable with the level of the primordial signal ($a = 1$ and $p = 1$) then the rate of clusterization varies more clearly. From Figures 3 and 4 one can see that the influence of the noise leads to the deduction of

the rate of clusterization for the CMB polarization. For the anisotropy field there is a shift of the percolation level with the variation of the shape of the curve. That is in total agreement with the conclusions in refs. [23] and [24].

6 SUMMARY AND DISCUSSION

In this paper we discussed different methods of analysis of the properties of the CMB polarization.

We have compared local and non-local descriptions of the polarization with different expressions for the field functionals S and P (see Section 3) in the case of noisy data. We conclude that the optimal observational strategy strongly depends upon the properties of the noise. For sufficiently rare sources of noise on the sky, a measurement of the local quantities S and P (see Eqs. (7)), which are obtained by differentiation of the Stokes parameters, seems to be more favourable. However isotropic noise with zero average may be easier to suppress by taking an average value over part of the sky.

We established a classification of the singular points of the flux lines of the eigenvector $\boldsymbol{n}^{(+)}$ of the polarization (Stokes) matrix. We have found that there are three possible types of singularities at the points where the polarization vanishes: saddles, comets, and beaks. They are different from the singularities known in the standard theory of two-dimensional vector fields. The former, as is well known, are saddles, knots, and foci (even though the name 'saddle' is the same in both cases the behaviour of the flux lines is quite different). The reason for this difference is a square root singularity of the vector $\boldsymbol{n}^{(+)}$ at the point where the polarization vanishes.

It is shown that in the case of Gaussian primordial fluctuations (as predicted by inflationary cosmology) the saddles make up 50% of all singular points, beaks make up 5.2%, and comets make up 44.8%. Deviations from these numbers may signal deviations from a Gaussian nature of perturbations or may indicate the existence of non-Gaussian noise in observational data. We realize that measurement of the polarization near the points where it vanishes is a formidable observational problem. But the patterns on polarization maps created by the flux lines of $\boldsymbol{n}^{(+)}$ in the regions where the polarization is non-zero is to a large extent determined by the types of nearest singularities. Thus one may hope that measurements of polarization on the patches where it is sufficiently large would permit us to determine the singularity types.

Finally we have investigated the statistics of the anisotropy and polarization of CMB fluctuations on the sky using a numerical approach (more details see ref. [26]). We have shown that the cluster analysis of CMB maps of the anisotropy and the polarization leads to the specific behaviour of mean lengths of clusters. The numerical examples show that manifestation of the presence of non-Gaussian noise in primordial cosmological signals of anisotropy and polarization depends very sensitively on the character of the noise. Note also that the simplest model of non-Gaussian noise in the anisotropy and polarization, discussed in Section 5.2, leads

to very broad variations of the mean length of a cluster, if the parameters a and p increase from $a, p = 0.04$ to $a, p \simeq 1$.

Acknowledgments

This work was supported in part by Danmarks Grundforskningsfond through its funding of the Theoretical Astrophysical Centre (TAC), the Danish Natural Science Research Council through grant No 9401635, in part by the Alexander von Humboldt Foundation and in part by grant INTAS 97-1192.

References

1 Hu, W. (1995) astro-ph/9508126.
2 Hu, W., Sugiyama, N., and Silk, J. (1997) *Nature* **386**, 37, astro-ph/9604166.
3 Bond, J. R. (1996) In: *Proc. of XXXI Moriond Conf.*, p. 471, astro-ph/9610119.
4 Zaldarriaga, M. (1998) astro-ph/9806122.
5 Lawrence, C. R., Scott, D., and White, M. astro-ph/9810446.
6 Hu, W. and White, M. (1997) *New Astronomy* **2**, 323.
7 Basko, M. A. and Polnarev, A. G. (1979) *Sov. Astr.* **24**, 3.
8 Polnarev, A. G. (1985) *Sov. Astr.* **29**, 607.
9 Bond, J. R. and Efstathiou, G. (1987) *Mon. Not. R. Astr. Soc.* **226**, 655.
10 Seljak, U. (1996) *Astrophys. J.* **482**, 6, astro-ph/9608131.
11 Seljak, U. and Zaidarriaga, M. (1997) *Phys. Rev. Lett.* **78**, 2054, astro-ph/9609169.
12 Zaidarriaga, M. and Seljak, U. (1997) *Phys. Rev. D* **55**, 1830, astro-ph/9609170.
13 Kamionkowski, M., Kosowsky, A., and Stebbins, A. (1997a) *Phys. Rev. Lett.* **78**, 2058, astro-ph/9609132.
14 Kamionkowski, M. and Kosowsky, A. (1998) *Phys Rev. D* **57**, 685, astro-ph/9705129.
15 Kamionkowski, M., Kosowsky, A., and Stebbins, A. (1997b) *Phys. Rev. D* **55**, 7368, astro-ph/9611125.
16 Seljak, U. and Zaidarriaga, M. (1998) astro-ph/9805010.
17 Kamionkowski, M. (1998) astro-ph/9803168.
18 Zaidarriaga, M. and Seljak, U. (1998) astro-ph/9810257.
19 Dolgov, A. D., Doroshkevich, A. G., Novikov, D. I., and Novikov, I. D. (1999b) *JETP Lett.* **69**, 427, astro-ph/9806104.
20 Efstathiou, G. and Bond, J. R. (1998) astro-ph/9807103, submitted to *Mon. Not. R. Astr. Soc.*
21 Naselsky, P. D. and Novikov, D. I. (1998) *Astrophys. J.* **501**, 31, astro-ph/9801285.
22 Naselsky, P. and Novikov, D. (1995) *Astrophys. J.* **444**, L1.
23 Novikov, D. and Jørgensen, H. (1996a) *Astrophys. J.* **471**, 1.
24 Novikov, D. and Jørgensen, H. (1996b) *Int. J. of Mod. Phys. D* **5**, 319.
25 Dolgov, A. D., Doroshkevich, A. G., Novikov, D. I., and Novikov, I. D. (1999a) *Int. J. of Mod. Phys. D* **8**, 189.
26 Arbuzov, P., Kotok, E., Naselsky, P., and Novikov, I. (1999) *Int. J. of Mod. Phys. D* **6**, 409.
27 Stebbins, A. (1996) astro-ph/9609149.
28 Gradshtein, I. S. and Ryzhik, I. M. (1994) *Tables of Integrals, Series, and Products*, Academic Press, Moscow.
29 Bronshtein, I. N. and Semendyaev, K. A. (1955) *Spravochnik po Mathematike* (in Russian), Gostechizdat, Moscow (English translation: (1998) *Handbook of Mathematics*, Springer-Verlag, Berlin, Heidelberg).
30 Mecke, K. R. and Wagner, H. (1991) *J. Stat. Phys.* **64**, 843.